EVALUATION OF HIGH DYNAMIC RANGE PHOTOGRAPHY AS A LUMINANCE MAPPING TECHNIQUE

Mehlika Inanici, Jim Galvin
December 2004

Lighting Research Group
Building Technologies Department
Environmental Energy Technologies Division
Lawrence Berkeley National Laboratory

Table of Contents:

Abstract:

The potential, limitations, and applicability of the High Dynamic Range (HDR) photography technique is evaluated as a luminance mapping tool. Multiple exposure photographs of static scenes are taken with a Nikon 5400 digital camera to capture the wide luminance variation within the scenes. The camera response function is computationally derived using the Photosphere software, and is used to fuse the multiple photographs into HDR images. The vignetting effect and point spread function of the camera and lens system is determined. Laboratory and field studies have shown that the pixel values in the HDR photographs can correspond to the physical quantity of luminance with reasonable precision and repeatability.

1. **Introduction:**

Through traditional measuring devices, it possible to measure the photometric information point by point. However, these measurements take a long time; are prone to errors due to measurement uncertainties in the field; and the obtained data may be too coarse for analyzing the lighting distribution and variation. There is a need for a tool that can capture the luminance values within a large field of view at high resolution, in a quick and inexpensive manner.

Photography has a potential for this kind of data collection. Photograph-based photometry is not a new approach; a number of researchers have utilized film-based photographs and CCD outputs for luminance measurements. A literature survey of early studies can be found in [1]. The common approach in most of these studies is to acquire the calibration functions for a certain camera and illuminant, which involves lengthy and complex physical measurements performed at laboratory conditions accompanied with extended data analysis [1, 2]. RGB values are converted to the CIE tristimulus values through these calibration functions. These early studies are based on single photographs, which provide quite a limited dynamic range of luminance values. More recent techniques, such as [3], employ multiple photographs, which allow capturing a larger luminance range. Some of these techniques require expensive equipment. All of these

studies require costly and tedious calibration processes, and yield calibration functions that are strictly device dependent.

In HDR Photography, multiple exposure photographs are taken to capture the wide luminance variation within a scene. The camera response function is computationally derived from these multiple exposure photographs; and then it is used to fuse these photographs into a single HDR image. HDR photography is not specifically developed for lighting measurement purposes. Therefore, it is necessary to evaluate the appropriateness (i.e. reasonable accuracy, applicability, and limitations) of the technique for lighting research. The specific objectives of the study are to:

- evaluate whether the pixel values in an HDR photograph correspond to the physical quantity of luminance with reasonable accuracy and repeatability;
- evaluate the effect of spectra on the accuracy;
- determine the camera/lens system's luminance vignetting (light fall-off) function for the fisheye lens
- determine the camera/lens system's point spread function (PSF).

2. Equipment and Software:

2. 1 Equipment:

The multiple exposure photographs are taken with a Nikon Coolpix 5400 digital camera with a fisheye lens (Nikon FC-E9) that is mounted on a tripod. The fisheye has 5.6 mm focal length, 190 angle of view, and equidistant projection properties. Reference physical measurements have been taken with a calibrated hand held Luminance meter with 1/3° field of view (Minolta LS110).

2.2 Software:

The photographs are fused into a HDR image using the software called Photosphere [4]. All photographs are taken with the camera settings shown in Table 1. It is especially

important to fix the white balance and contrast settings for achieving consistent color space transitions. Changing either the aperture size (f-stop) or the shutter speed (exposure time) can vary the exposure values. In this study, exposure variations are achieved with a fixed aperture size, and varying only the shutter speed. Shutter speed is a more reliable measure than aperture size in changing the exposure values [5, 6]. After a preliminary study on various aperture sizes, we have decided to use a fixed aperture size at f/4.0 and varied the exposure in manual exposure mode (2 to 1/4000 sec).

Table 1. Camera settings

Feature	*Setting*	*Feature*	*Setting*
White Balance	Daylight	Image Size	2592 x 1944
Best Shot Selector	Off	Sensitivity	100 ISO
Image Adjustment	Normal	Image Sharpening	Off
Saturation Control	Normal	Lens	Fisheye
Auto-bracketing	Off	Noise Reduction	Off

Photosphere generates the camera response curve based on multiple exposure sequences. To determine the camera's natural response function, it is suggested to select an interior scene with daylight that has large and smooth gradients throughout the interior and exterior views [7]. Many different scenes have been comparatively studied for the camera response curve. For each scene, 10 or more exposure sequences are recorded. The camera response function for the Nikon 5400 that is being using in this study is computationally determined in three channels (RGB) as follows (Fig. 1):

$$R = 1.53994x^3 - 0.99492x^2 + 0.46536 - 0.01037$$
$$G = 1.31795x^3 - 0.69784x^2 + 0.38994 - 0.01005$$
$$B = 1.67667x^3 - 1.09256x^2 + 0.42334 - 0.00745$$

The curves are polynomial functions that model the accumulated radiometric non-linearities of the image acquisition process (such as gamma correction, A/D conversion, image digitizer, various mappings, without addressing the individual source of each non-linearity). This technique, known as the radiometric self-calibration [5], is a computationally derived calibration process that is used to relate the pixel values to the real-world luminances. The HDR images can be stored in image formats such as

Radiance RGBE [8] and LogLuv TIFF [9], where the pixel values can extend over the luminance span of the human visual system (14 logarithmic units from 10^{-8} to 10^{6} cd/m^2).

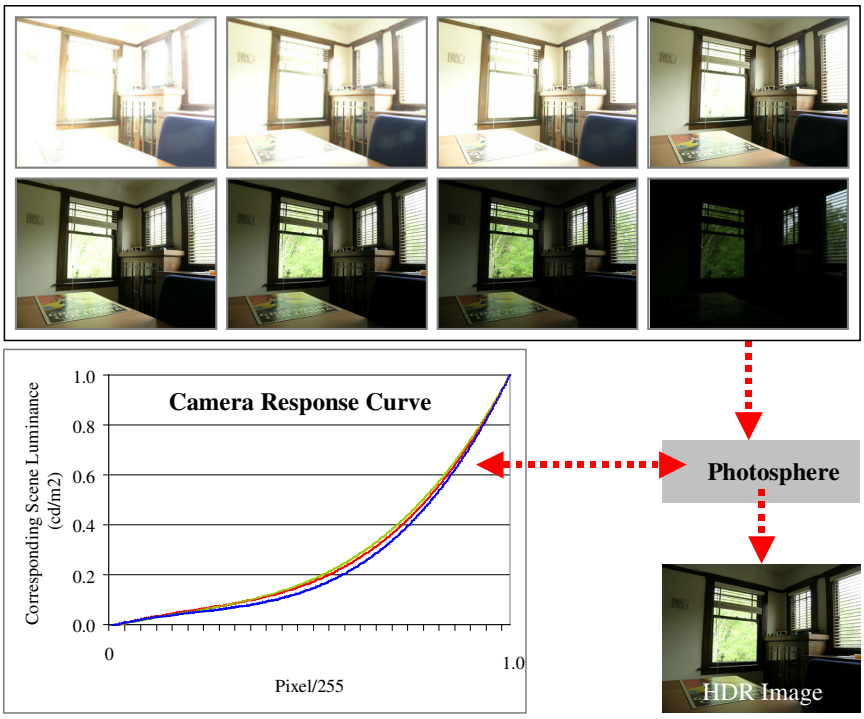

Fig. 1 The camera response curve for Nikon 5400 as determined by Photosphere

2.3 Luminance Calculation:

For analyzing the HDR images from Photosphere, computational procedures have been implemented (referred as HDRLab). The routines are written in Matlab® and they allow the user to extract and process per-pixel lighting data from the HDR Photographs that are saved in Radiance RGBE format. CIE XYZ values for each pixel are quantified from floating point RGB values based on the standard color space (sRGB) reference primaries [10], CIE Standard Illuminant D_{65}, and standard CIE Colorimetric observer with 2° field of view. The transformation process is illustrated in Fig. 2. It is possible to calibrate images and cameras in Photosphere with a physical luminance measurement of a selected region in the scene. This feature can be applied as a constant either to the pixel values in an image or to the camera response function.

Floating point RGB is calculated from RGBE integer values as follows [8]:

$$red = \frac{R}{255} * 2^{(Exponent-128)},\ green = \frac{G}{255} * 2^{(Exponent-128)},\ blue = \frac{B}{255} * 2^{(Exponent-128)}$$

CIE chromaticities for the reference primaries and CIE Standard Illuminant D65 are:

R (x, y ,z) = (0.64, 0.33, 0.03)

G (x, y, z) = (0.30, 0.60, 0.10)

B (x, y, z) = (0.15, 0.06, 0.79)

D_{65} (x, y, z) = (0.3127, 0.3290, 0.3583)

Conversion from RGB to XYZ: The RGB-to-XYZ matrix is constructed with the matrix of RGB chromaticities ('K'), which are differentially scaled to achieve the unit white point balance (denoted by 'W"). Further information on RGB-toXYZ conversion can be found in [11, 12].

$$K = \begin{bmatrix} r_x & r_y & r_z \\ g_x & g_y & g_z \\ b_x & b_y & b_z \end{bmatrix} = \begin{bmatrix} 0.64 & 0.33 & 0.03 \\ 0.30 & 0.60 & 0.10 \\ 0.15 & 0.06 & 0.79 \end{bmatrix}$$

$$W = \begin{bmatrix} \frac{X_n}{Y_n} & 1 & \frac{Z_n}{Y_n} \end{bmatrix} = \begin{bmatrix} 0.9505 & 1.0 & 1.0891 \end{bmatrix}$$

$$V = WK^{-1} = \begin{bmatrix} 0.6444 & 1.1919 & 1.2032 \end{bmatrix} = \begin{bmatrix} G_r & G_g & G_b \end{bmatrix}$$

$$G = \begin{bmatrix} G_r & 0 & 0 \\ 0 & G_g & 0 \\ 0 & 0 & G_b \end{bmatrix} = \begin{bmatrix} 0.6444 & 0 & 0 \\ 0 & 1.1919 & 0 \\ 0 & 0 & 1.2032 \end{bmatrix}$$

$$N = GK = \begin{bmatrix} 0.4124 & 0.2127 & 0.0193 \\ 0.3576 & 0.7151 & 0.1192 \\ 0.1805 & 0.0722 & 0.9505 \end{bmatrix} = \begin{bmatrix} X_r & X_g & X_b \\ Y_r & Y_g & Y_b \\ Z_r & Z_g & Z_b \end{bmatrix}$$

$$X = 0.4124 * R + 0.3576 * G + 0.1805 * B$$
$$Y = 0.2127 * R + 0.7151 * G + 0.0722 * B$$
$$Z = 0.0193 * R + 0.1192 * G + 0.9505 * B$$

In calculating luminance (L), CIE Y is multiplied by a constant value 'k', where k can be either a constant for the camera or determined for a scene based on a measurement of a selected region in the scene.

$$L = k * (0.2127 * R + 0.7151 * G + 0.0722 * B) \qquad (cd/m^2)$$

Fig. 2 Conversion from RGBE to XYZ

3. Measurement Setups and Analyses:

The measurement process involves the comparison of luminance values of various surfaces as determined from HDR images and the luminance meter. The measurements have been repeated in different settings, which varied from controlled laboratory environments (black painted room without daylight) to office spaces and outdoors. The interior settings involve different light sources and different illumination levels. Caution has been taken so that the equipment and the people who make the measurements do not cast shadows on the targets. The measurements are done with 5 sets of paper targets: The first target consists of 24 squares (two sets of 12 squares) that have reflectances ranging between 4-87%. The other four targets have a gray square target in the middle with a 28% reflectance. This square is enveloped by a) white (87% reflectance); b) black (4%); c) white-then-black d) black-then-white surroundings (Fig. 3). The Macbeth ColorChecker® chart is also used as a target.

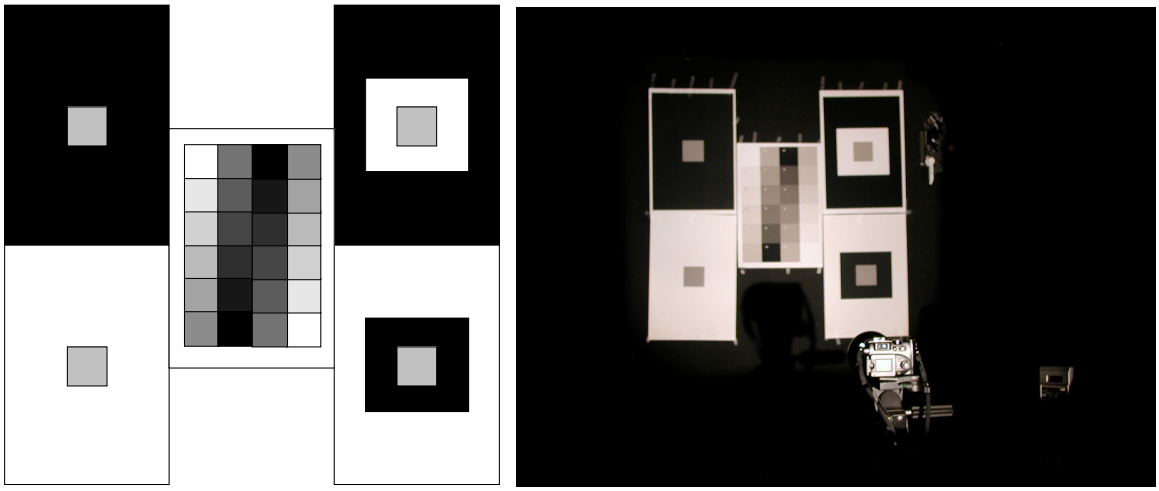

Fig 3. Arrangement of the grayscale targets, and the measurement set-up

The center of each target is measured with the Minolta luminance meter. When daylight was present in the setup, the physical measurements were done twice: before and after the multiple exposure photographs were taken. There is a time lag between the physical measurements and the multiple exposure photographs sequential; therefore bracketing the

photograph sequential with physical measurements allows us to characterize the variation of the lighting conditions during the tests. Each measurement setup is also captured with the HDR photographs. A rectangular block of pixels is extracted from the digital image for each target. This size of the block varies depending on the resolution of the target such that the selection area fits inside each target and excludes the borders, where the luminance values may change drastically. The minimum, maximum, mean, and standard deviation of each block has been studied to ensure that the luminance values do not change significantly within the selected region. This approach is more reliable than processing 1 or 2 pixel values.

3.1 Accuracy

Figures 4-18 illustrates various experimental setups and the luminance value comparisons between the HDR photography and physical luminance meter. A laboratory space (Fig. 4) is illuminated with different light sources such as incandescent lamp, projector (using a 500W tungsten lamp), fluorescent, metal halide (MH), and high pressure sodium (HPS) lamps. Figures 5- 11 show the accuracy results for these light sources. Figures 12-15 show different office spaces illuminated with daylight and electric lighting. Figures 16-18 illustrate outdoor scenes with dynamic lighting conditions.

Fig. 4 The laboratory space illuminated with different light sources: the accuracy tests are carried out with Target 1 and Macbeth ColorChecker® chart

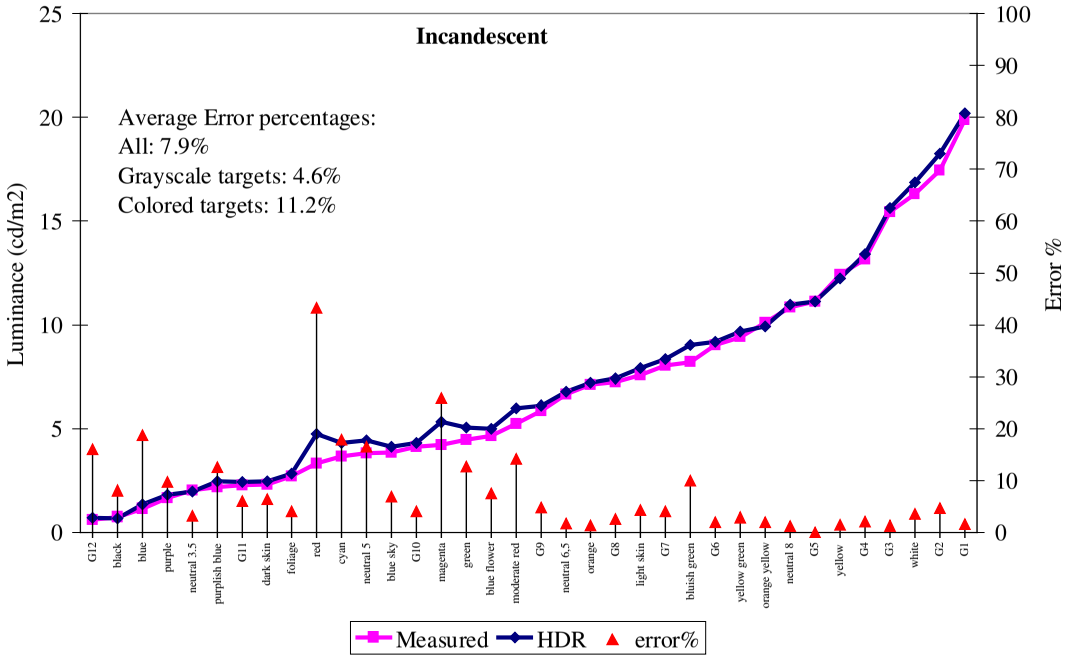

Fig. 5 Dark room with grayscale and colored targets, illuminated with incandescent lamp

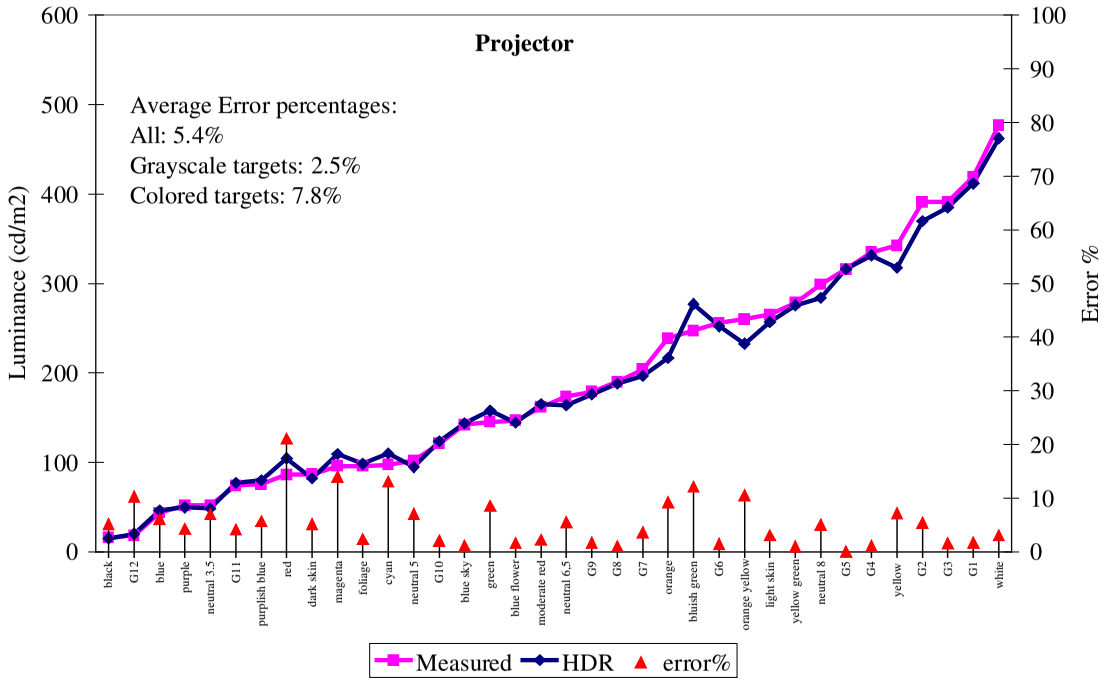

Fig. 6 Dark room with grayscale and colored targets, illuminated with a projector

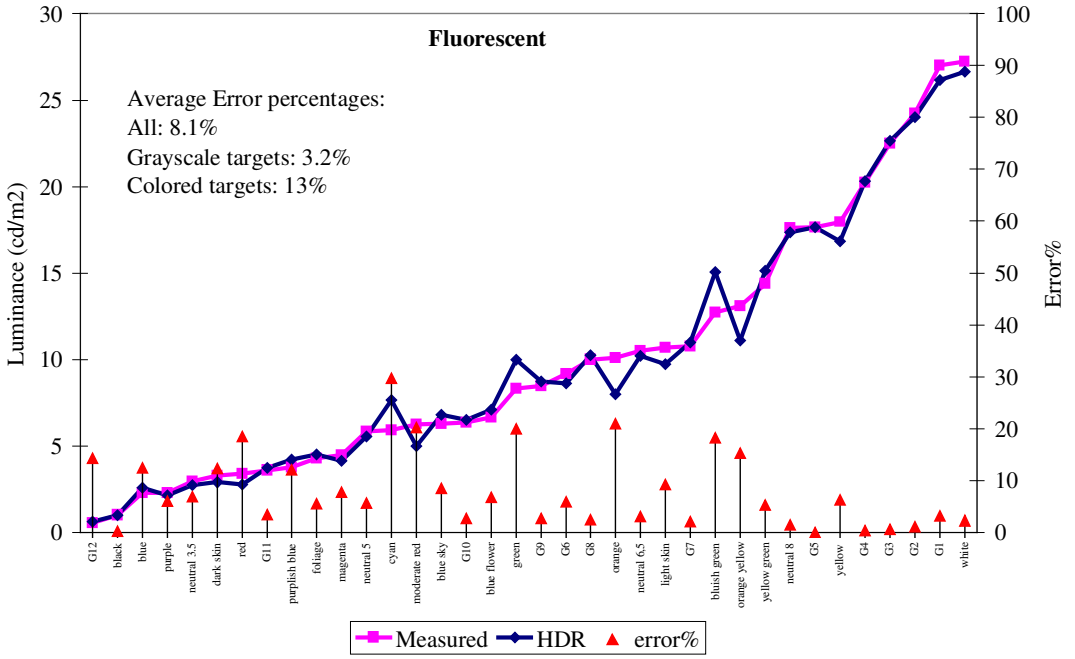

Fig. 7 Dark room with grayscale and colored targets, illuminated with a T12 fluorescent (6500K) lamp

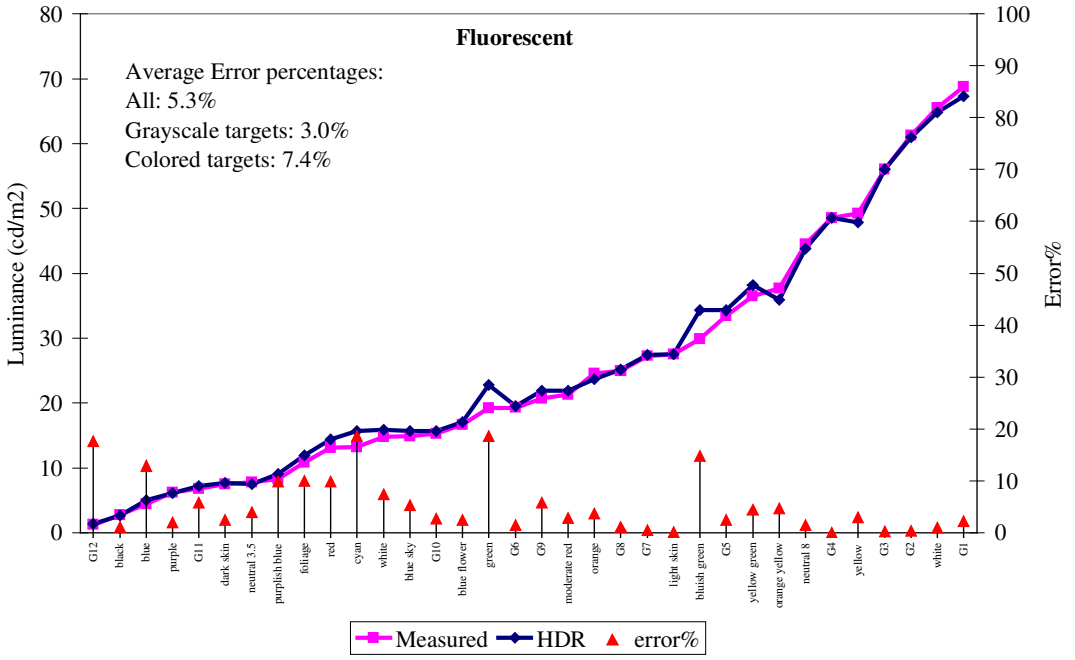

Fig. 8 Dark room with grayscale and colored targets, illuminated with a T8 fluorescent (3500K) lamp

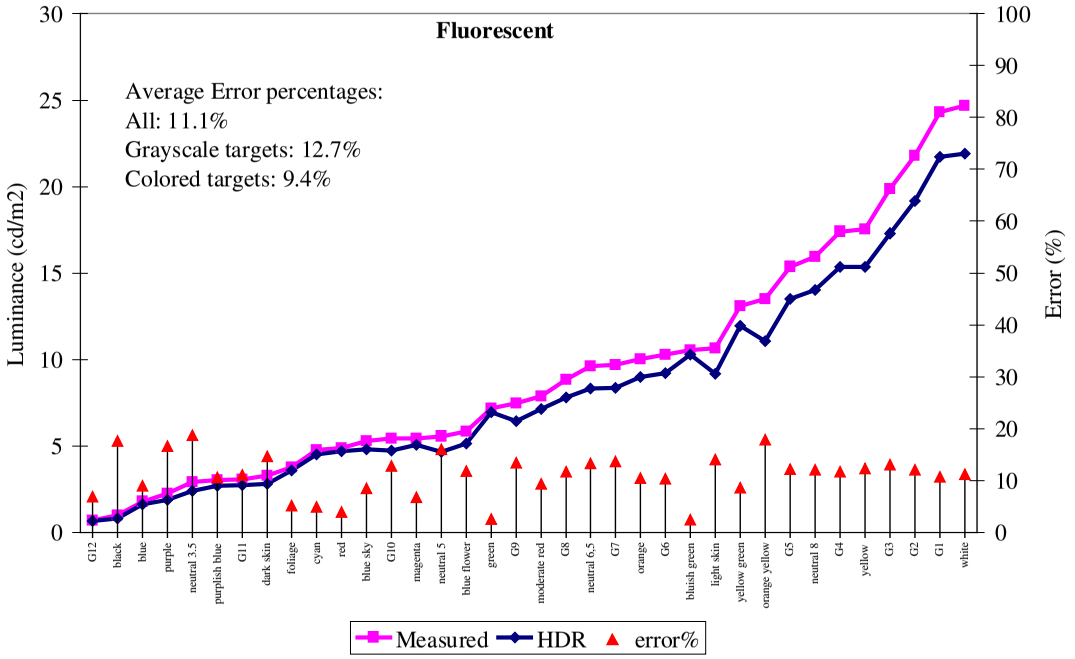

Fig. 9 Dark room with grayscale and colored targets, illuminated with a T5 fluorescent (3000K) lamp

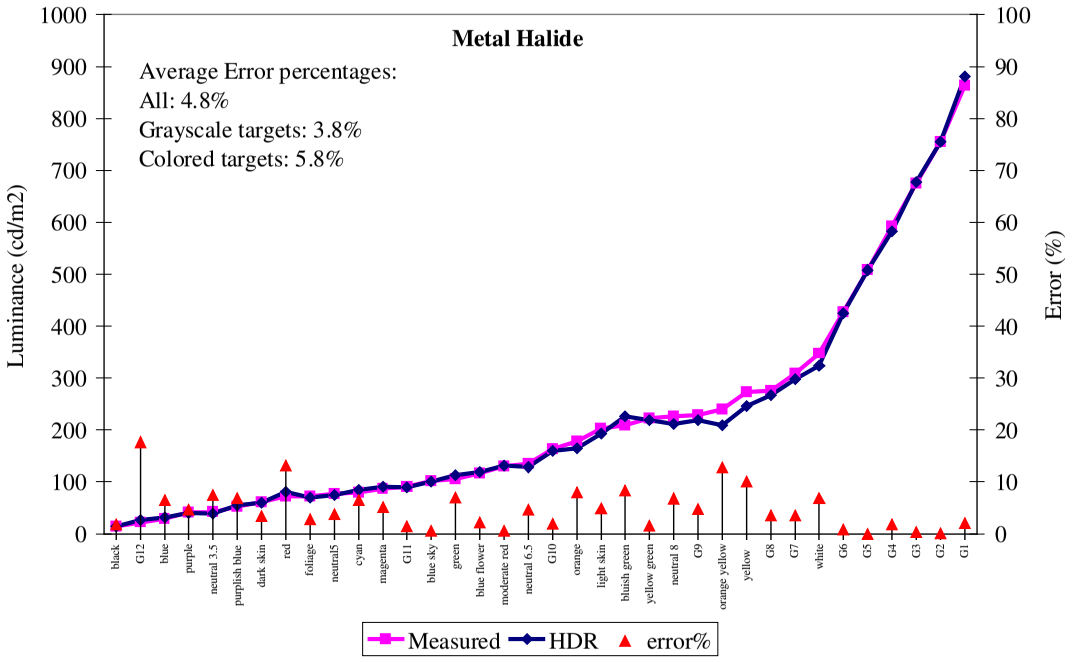

Fig. 10 Dark room with grayscale and colored targets, illuminated with a metal halide lamp

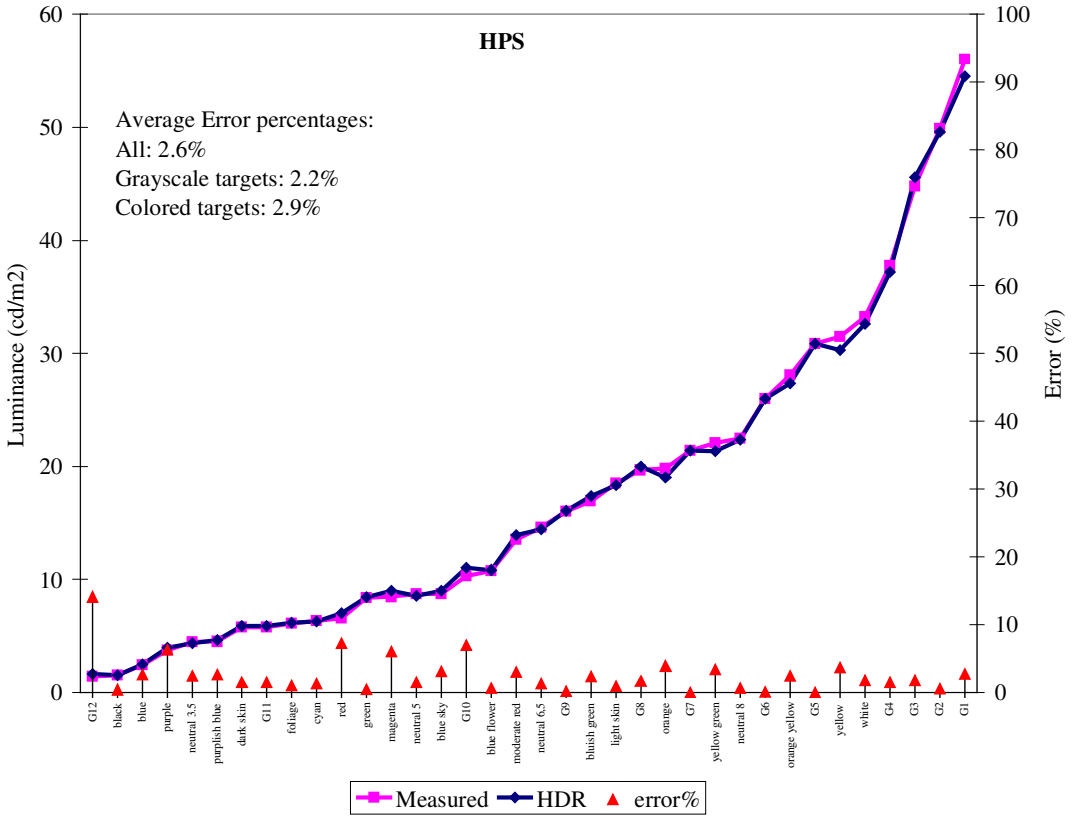

Fig. 11 Dark room with grayscale and colored targets, illuminated with a HPS lamp

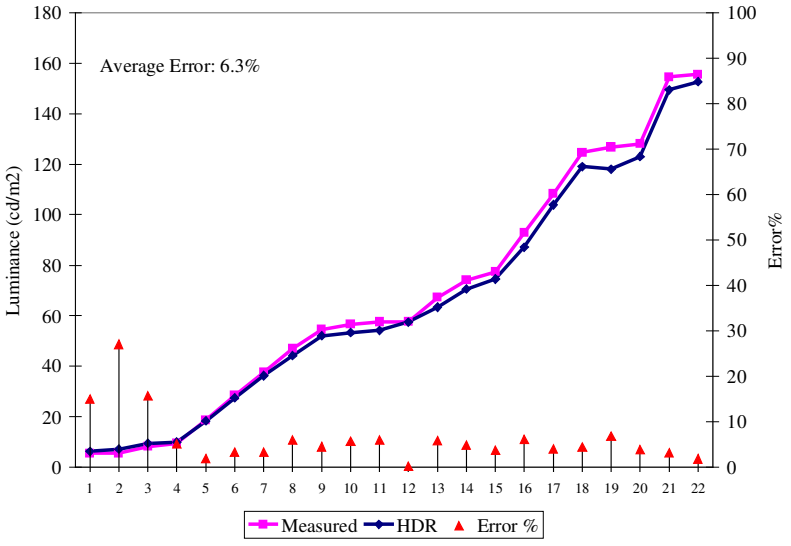

Fig. 12 Grayscale targets in an office space with daylighting and electric lighting

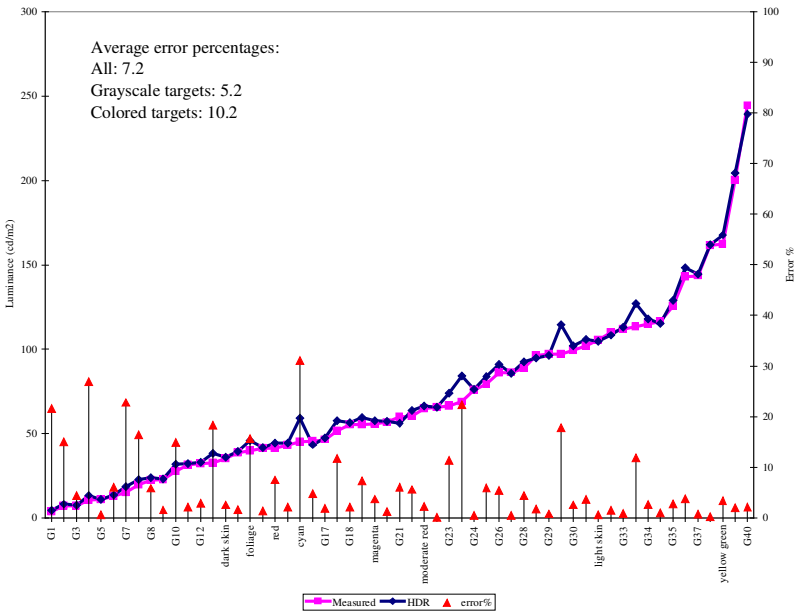

Fig. 13 Colored and grayscale targets in an office space with daylighting and electric lighting

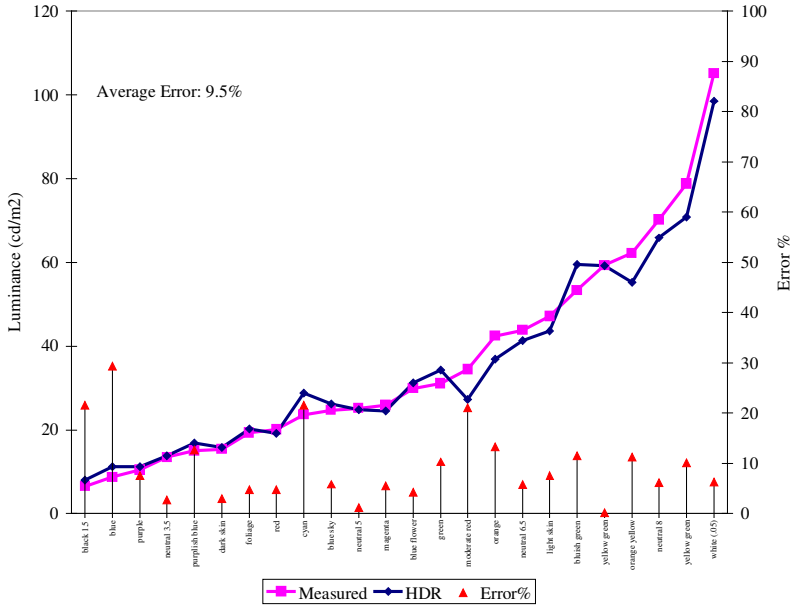

Fig. 14 Colored targets in an office space with daylighting and electric lighting (Average error percentage is 9.5).

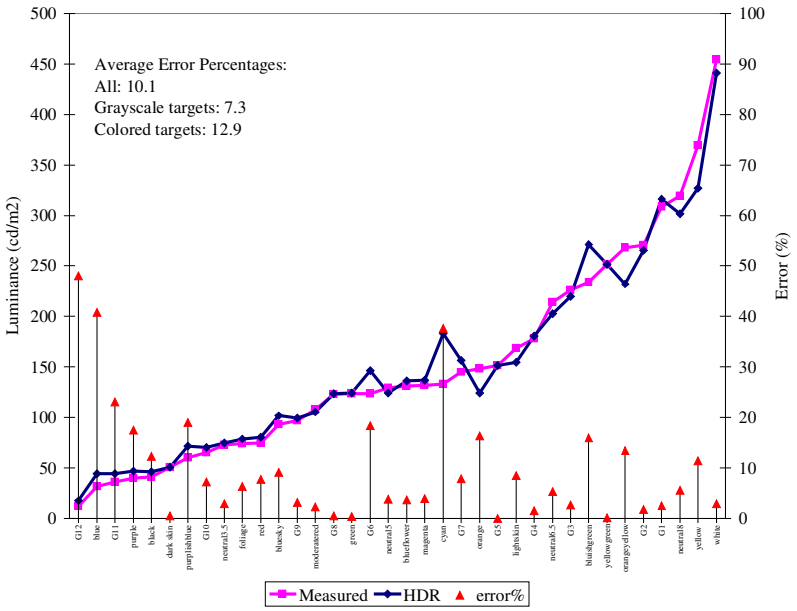

Fig. 15 Office space with daylighting

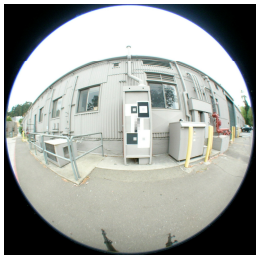

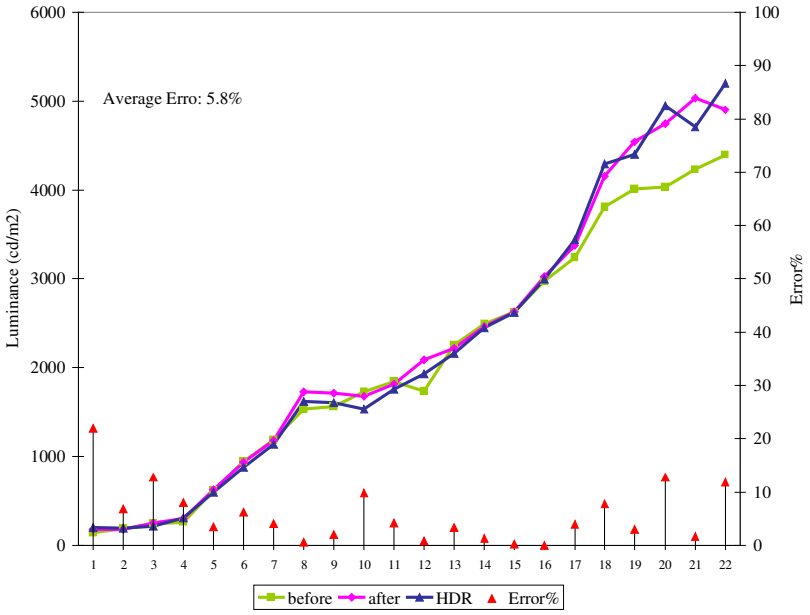

Fig. 16 Outdoor scene with grayscale targets under overcast sky

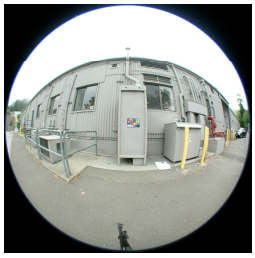

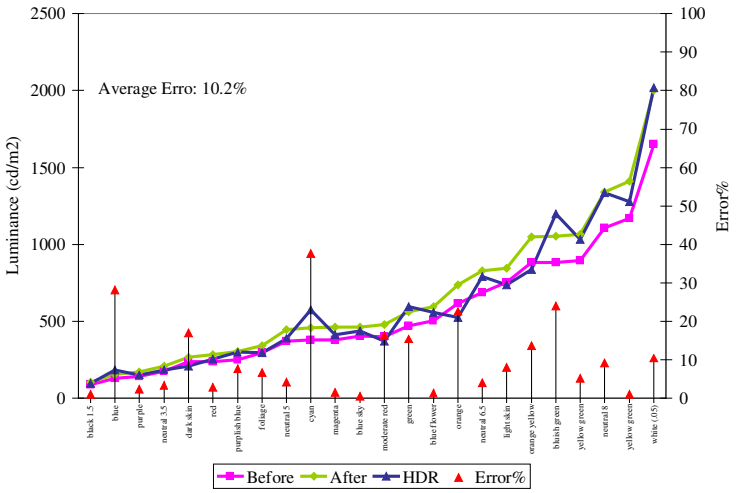

Fig. 17 Outdoor scene with colored targets under overcast sky

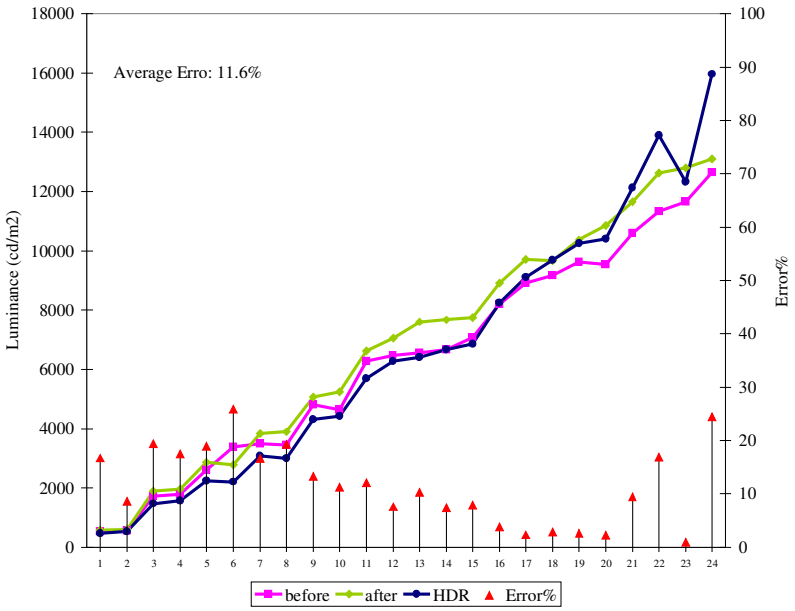

Fig. 18 Outdoor scene with grayscale targets under sunny sky

3.2 Spectra

The accuracy of the HDR photography has been evaluated in relation to the spectra of the light source. Fig. 19 demonstrates the spectra of the light sources that are shown in Fig. 5-11, as they are measured with an OceanOptics Spectrophotometer. The spectral properties of the light sources are quite different. The error margins for grayscale and colored targets vary depending on the spectral power distribution of the light sources. Yet, the accuracy has proven to be reasonable (error margin within 10%) for all targets (Fig. 20).

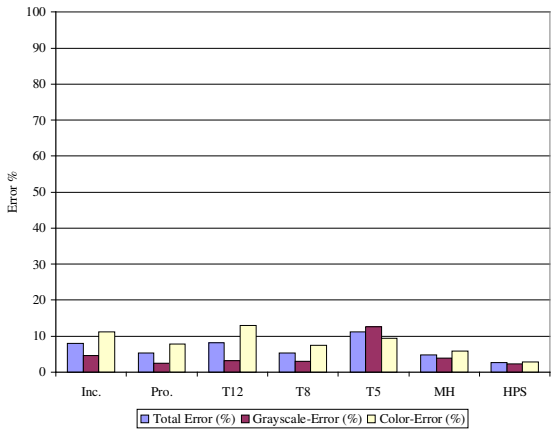

Fig. 20 Error percentages for different light sources (from Fig. 5-11).

3.3 Vignetting – Light falloff

The Nikon FCE9 fisheye lens uses equidistant projection to produce an image (Fig. 21). As opposed to orthographic projection, equidistant fisheye lenses exhibit noticeable light falloff (which will be referred as vignetting, here after) for the pixels far from the optical axis. It is therefore necessary to address this problem. The approach adopted is to determine the vignetting function of the Nikon FCE9 fisheye lens and use this function to devise a 'digital filter' in HDRLab to compensate for the luminance loss.

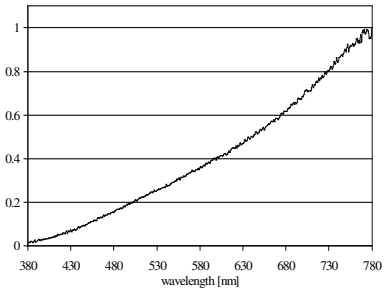

Incandescent (2850 K)

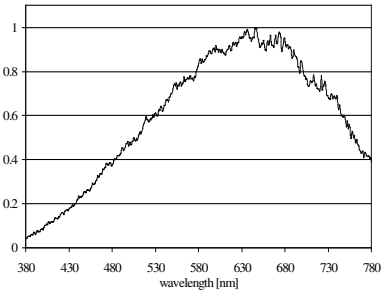

Projector (3300 K)

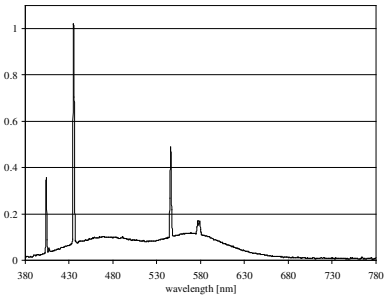

Fluorescent –T12 (6500)

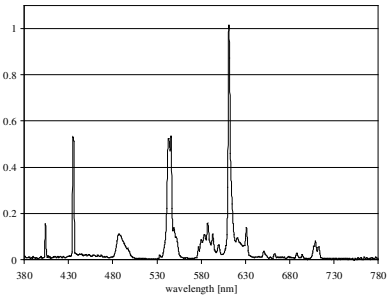

Fluorescent – T8 (3500)

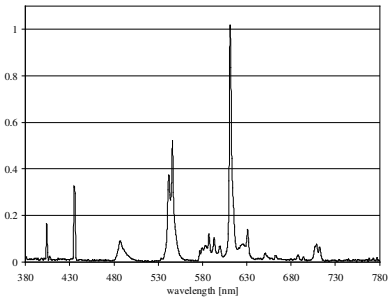

Fluorescent-T5 (3000 K)

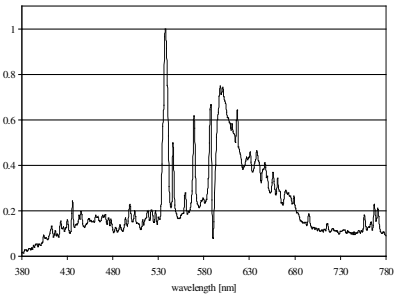

Metal Halide (3700 K)

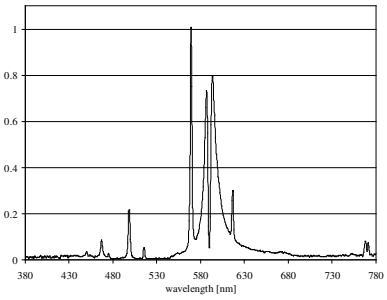

HPS (2500 K)

Fig. 19 Spectral properties of the different light sources utilized in accuracy measurements (Fig. 5-11).

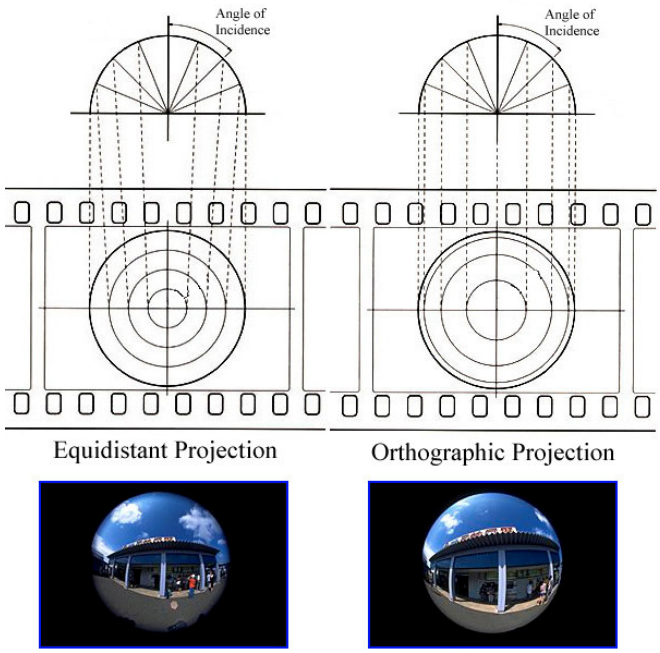

Fig. 21. Comparison of a equidistant and orthographic fisheye projections [13]

The digital vignetting filter is applied to all images as a post-process. Two different experiments have been conducted to assure an accurate vignetting function. In the first experiment, the targets are arranged at known intervals (Fig. 22a). The measured and captured luminance values are compared to derive the vignetting function. In a subsequent experiment, one target is used in a laboratory environment, and the camera has been rotated with respect to the target in 5° intervals until the camera field of view has been covered (Fig. 22b).

Both experiments yielded similar results, though the second experiment has provided a smoother function. Fig. 23a illustrates the measured data points (5° intervals as the camera is rotated) and the function derived from the data points. As it can be seen from the figure, vignetting effects are insignificant in the center of the image and the maximum effect is at the periphery with 23% luminance loss. The vignetting effect is calculated as a polynomial function as follows (x corresponds the pixel location):

$$y = -1.28\text{E-}12 * x^4 + 3.43\text{E-}09 * x^3 - 3.38\text{E-}06 * x^2 + 1.45\text{E-}03 * x + 7.70\text{E-}01$$

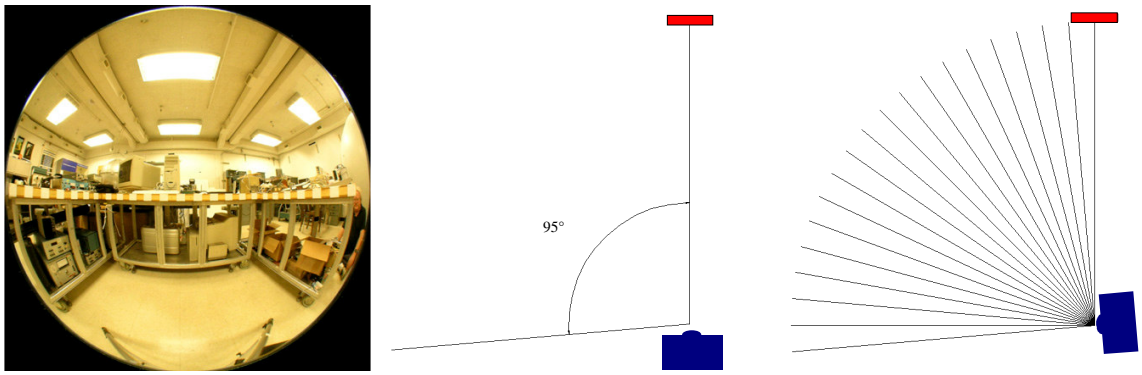

(a) (b)

Fig. 22 The experimental setups for determining the vignetting function for the Nikon EC-9 fisheye lens a) the targets are arranged at known intervals and camera position is kept constant b) target is kept constant and camera is rotated at 5° intervals.

Note that vignetting fall-off is strongly dependent on the aperture size, and increases dramatically with wider apertures. The function is generated for an aperture size of f/4.0. The square of the correlation (r^2) between the measured points and the derived vignetting function is 99.12%. Fig. 23b is the digital filter developed in HDRLab based on the vignetting function. This filter is a matrix that has the same resolution as the fisheye image and it compensates for the vignetting effect in the image based on the pixel locations.

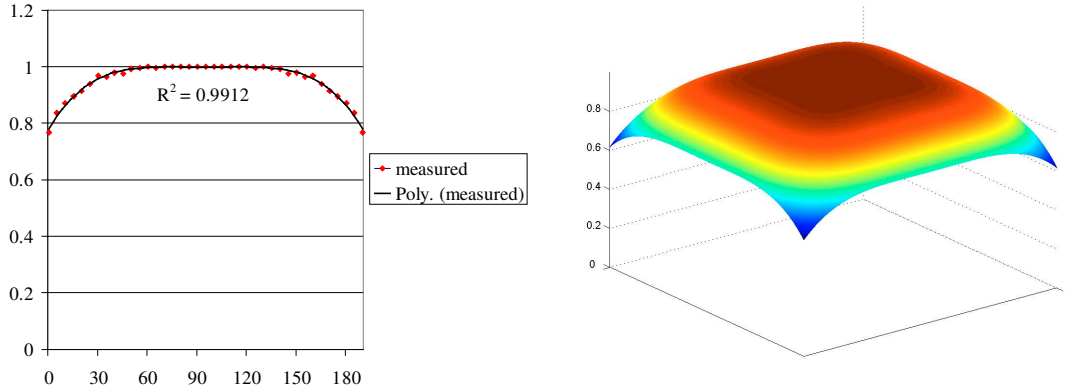

(a) (b)

Fig. 23 The vignetting function of Nikon FC9 a) measured data points b) digital filter developed based on the vignetting function derived from (a)

3.4 Point spread function

It would have been very convenient to interpret each pixel in the photograph as a luminance measurement, but unfortunately, in most optical systems some portion of the pixel signal comes from surrounding areas. Light entering the camera is spread out and scattered by the optical structures of the lens, which is referred as the point spread function (PSF) [14].

A small point light source is used to quantify the PSF. The source is located far enough such that it covers less than one pixel area. Without any point spread, the image of the light should be equal to the original point of light, i.e. one pixel. The point spreading is illustrated in Fig. 24 as a close-up view.

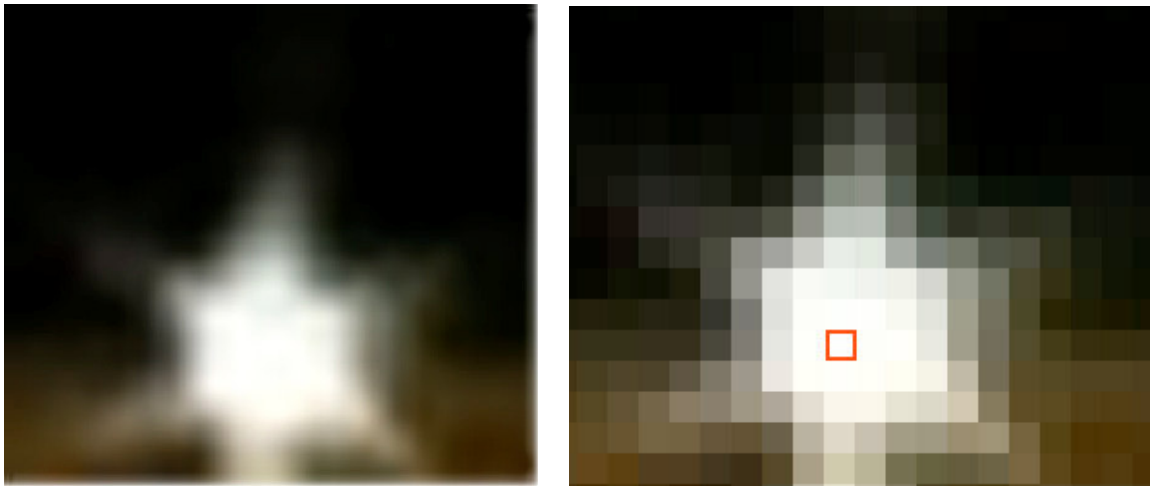

Fig. 24 Close-up views of point spreading: the red rectangle in the right figure shows the pixel that corresponds to the actual light source.

The aperture size, exposure time and eccentricity (distance from the optical center) affect PSF. The aperture size is kept constant throughout the capturing processes; therefore it is not a parameter affecting the luminance values. The effects of exposure time and eccentricity are recorded and they are plotted in RGB channels. The PSF for differently exposure photographs and the PSF in the resultant HDR image are shown in Fig. 25 and 26, respectively. The effect of the eccentricity is studied in 15° intervals and it is illustrated in Fig. 27. The spread is affecting a limited number of the neighboring pixels.

For most architectural lighting applications, it seems to be a small effect. However, it is important to note that the general scattering of light, such that the cumulative effect of a bright background surrounding a dark target, can lead to larger measurement errors. This is indeed evident in the measurement results of darker targets shown in Part 3.1. Unfortunately, it is not feasible to quantify the general scattering. The consequence is an error margin, quantified as less than 10% on average. The user should take this effect into account for interpreting the pixel values under relevant conditions.

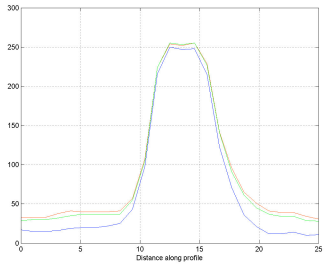

Exposure time: 2 sec

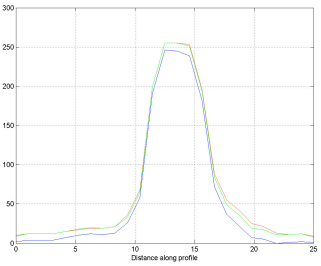

1 sec

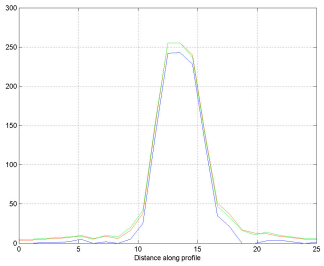

1/2 sec

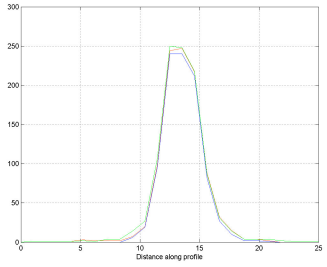

1/4 sec

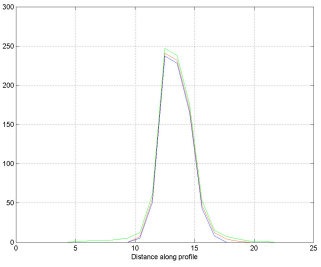

1/8 sec

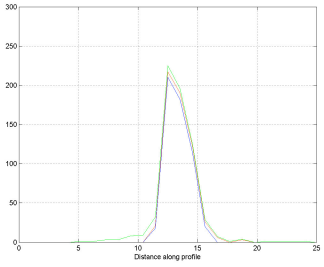

1/15 sec

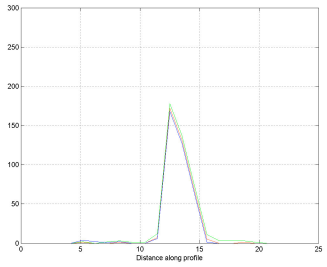

1/30 sec

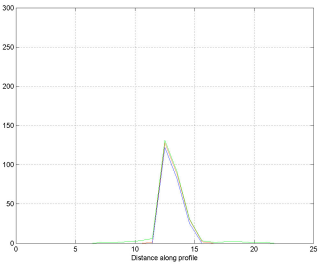

1/60 sec

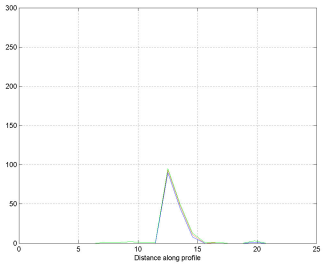

1/125 sec

Fig. 25 PSF as a function of exposure time

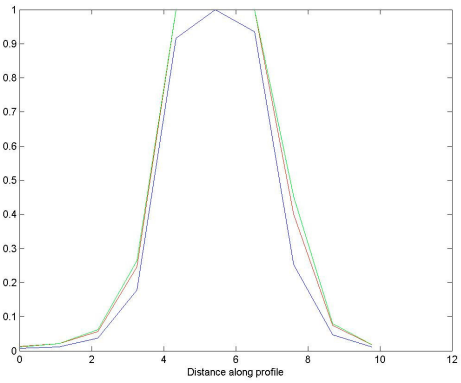

Fig. 26 PSF in the HDR image constracted from the exposure times shown in Fig. 25.

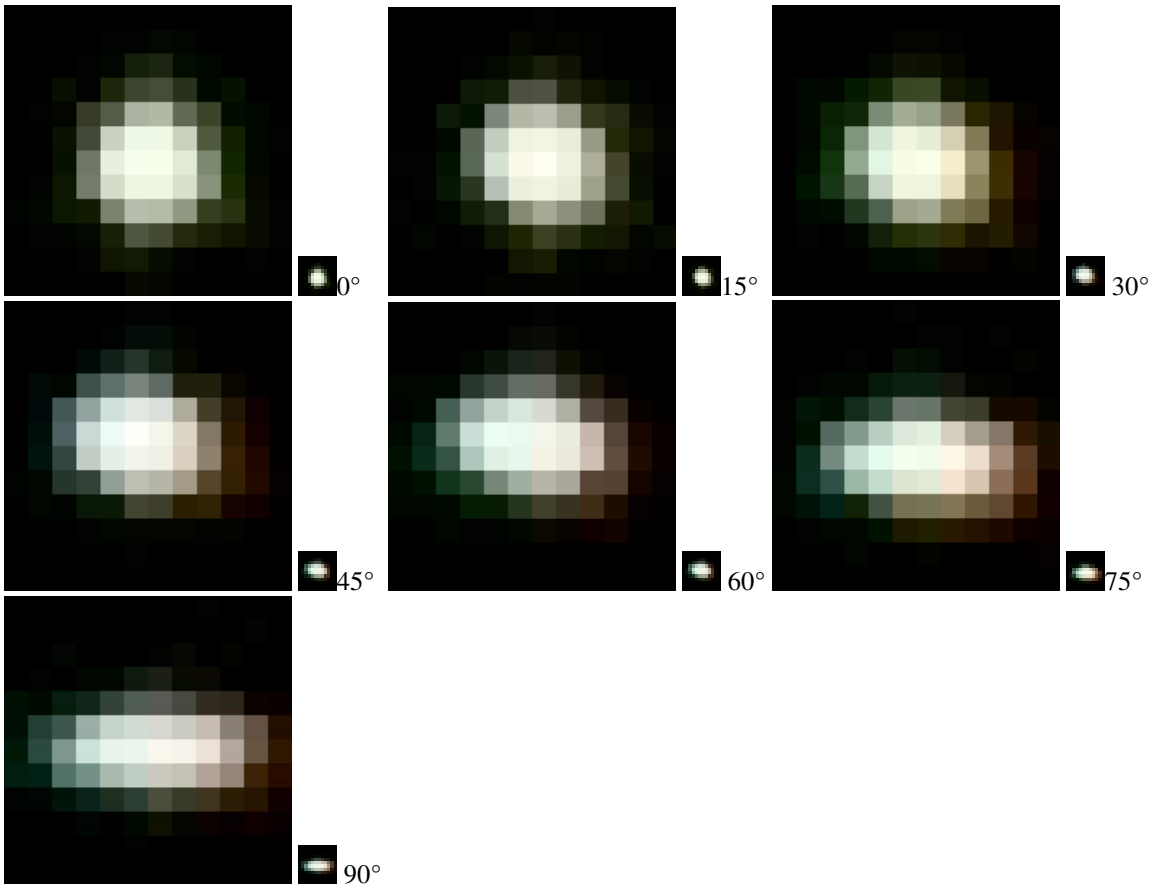

Fig. 27 PSF as a function of eccentricity (distance from the optical center) in the camera field of view

4. Discussion

The HDR images used in this paper are gnerated with the camera response functions shown in Fig. 1. The luminance values are calculated with the transformation functions given in Fig. 2. The calibration feature of Photosphere is used for fine tuning the luminance values with one of the gray targets in the scene. The vignetting effect is corrected by utilizing the function shown in Fig. 23.

The luminance values extracted from the HDR photographs indicate reasonable accuracy when compared with physical measurements. Fig. 28 presents a histogram for error percentages for the 485 target points from different scenes (Fig. 5-18). Therefore, it involves a wide range of conditions with various light sources including daylight and electric lights, and various targets including colored and grayscale objects. The minimum and maximum measured target luminances are 0.5 and 12,870 cd/m^2. The average error percentages for all, grayscale, and colored targets are 7.3, 5.8, and 9.3, respectively. The square of the correlation (r^2) between the measured and captured luminance values is found to be 98.8%.

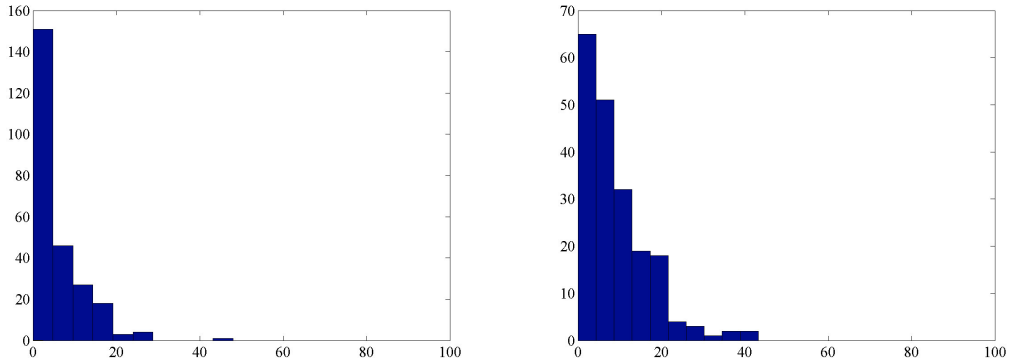

(a) (b)

Fig. 28 Histograms for error percentages between the measured and captured luminance values for a) grayscale targets b) colored targets

There is an increased error for the darker grayscale targets. As mentioned in Section 3.4, the general scattering in the lens and sensor affects the darker regions of the images disproportionately. The consequence is the over-estimation of the luminance values of the darker regions. Since the luminance level is quite low for these targets, small differences between the measured and captured values yield to higher error percentages.

The results also revealed increased errors for the saturated colors (Fig. 28b). In Photosphere, a separate polynomial function is derived fit to each RGB channel. However, it is important to note that the RGB values produced by the camera have been mixed between the different red, green, and blue sensors of the CCD. The CCD sensors have colored filters that pass red, green, or blue light. With the large sensor resolution, it is assumed that enough green (or, red, or blue)-filtered pixels receives enough green (or, red, or blue) light that the image would yield reasonable results. The sensor arrays are usually arranged in a Bayern (mosaic) pattern such that 50% of the pixels have green and 25% of the pixels have red and blue filters. When the image is saved in a file (such as JPEG), algorithms built within the camera employ interpolation between the neighboring pixels [15]. The HDR algorithm assumes that the computed response functions preserve the chromacity of the corresponding scene points [5]. In an effort to keep the RGB transformations constant within the camera, the white balance setting is being kept constant throughout the capturing process. The camera response functions are generated with these constraints. Likewise, the luminance calculations are approximated based on sRGB reference primaries, with the assumption that sRGB provides a reasonable approximation to the camera sensor primaries.

The HDR photography technique is a useful tool that can capture HDR luminance values overall within 10% accuracy over a wide range of luminances. It is worth mentioning that physical measurements also have expected errors: V(λ) match (3%), UV response (0.2%), IR response (0.2%), directional response (2%), effect from the surrounding field (1%), linearity error (0.2%), fatigue (0.1%), polarization (0.1%), and errors of focus (0.4%). The percentage values are published by the CIE [16] and they correspond to representative errors that are collected from the best available commercial instruments.

The expected error total is 7.2%. HDR photography is not a substitute for physical measurements. It is not as accurate as physical measurements. Yet, it provides a measurement capability with the advantage of collecting high-resolution luminance data within a large field of view quickly and efficiently, which is not possible to achieve with a physical luminance meter. It uses affordable equipment that is within the budgets of advanced lighting practitioners and researchers. Additionally, the self-calibration algorithm in Photosphere provides quick and easy camera response functions compared to the lengthy calibration measurements required in prior research. An HDR image can be:

1) post-processed to
    - extract photometric information on a pixel scale; this information can be utilized for statistical and mathematical analysis;
    - generate false-color image and/or iso-contour lines (Fig. 29);
    - simulate human visual sensitivity through a tone mapping operator ;
2) studied for visual analysis by adjusting the exposure to different ranges; and
3) used for presentation.

The HDR technique requires reasonably stable conditions over the period of measurements. Dynamic lighting conditions resulting in significant light changes between differently exposed photographs can compromise the accuracy of the end result. Since the main application of these images is research, high accuracy is a major objective. Therefore, it is advisable to measure a single target in the scene, to be used as a calibration feature. Finally, as with any measurement and simulation tool, the user should be aware of the limitations and expected errors to be able to interpret the results meaningfully.

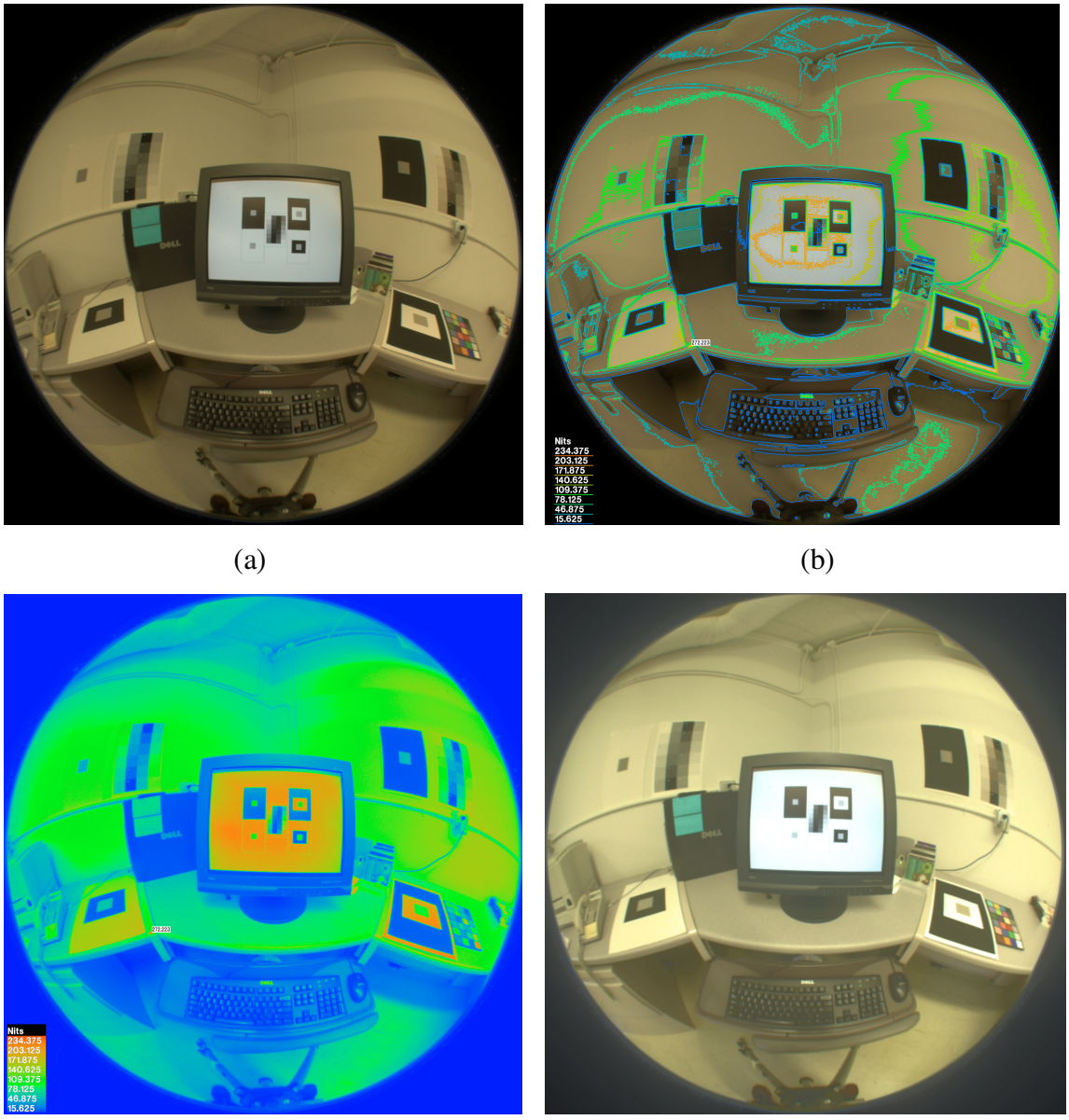

Fig. 29 a) HDR image b) iso-contour lines showing luminance distribution c) false color image showing luminance distribution d) simulated human vision

ACKNOWLEDGEMENTS:

This work was supported by the Assistant Secretary for Energy Efficiency and Renewable Energy, Office of Building Technology, Building Technologies Program, of the U.S. Department of Energy under Contract No. DE-AC03-76SF00098. The authors

thank to Greg Ward (Anyhere Software) for his continuous comments and feedback throughout the study, and to Steve Johnson (LBNL) and Francis Rubinstein (LBNL) for their suggestions.

REFERENCES

[1] Uetani, Y. "Measurement of CIE Tristimulus Values XYZ by Color Video Images – Development of Video Colorimetry", *Journal of Architecture, Planning, and Environmental Engineering*, 2000.

[2] Belia L, Minichiello F, and Sibilio S. "Setting up a CCD photometer for Lighting Research and Design", *Building and Environment*, 37(11), Nov. 2002, 1099-1106.

[3] Coutelier, B. and Dumortier, D. "Luminance Calibration of the Nikon Coolpix 990 Digital Camera" *International Commission on Illumination (CIE) 2003 Conference*, San Diego, 26 - 28 June, 2003.

[4] Ward, G. *Photosphere*, http://www.anyhere.com/.

[5] Mitsunaga, T. and Nayar, S.K. "Radiometric Self Calibration", *Proceedings of IEEE Conference on Computer Vision and Pattern Recognition*, Fort Collins, June, 1999.

[6] Debevec, P.E. and Malik, J. "Recovering high dynamic range radiance maps from photographs", *ACM SIGGRAPH Proceedings of the 24th Annual Conference on Computer Graphics and Interactive Techniques,* 1997, 369-378.

[7] Ward, G. *Photosphere Quick-start*, http://www.anyhere.com/

[8] Ward, G. "Real pixels". In *Graphics Gems II,* (Arvo, J. (ed)). Boston: Academic Press, Inc., 1991.

[9] Ward, G. "The LogLuv Encoding for Full Gamut, High Dynamic Range Images", *ACM Journal of Graphics Tools*, 3(1), 15-31, 1998.

[10] Stokes, M. and Chandrasekar, S. "Standard color space for the internet –sRGB", http://www.w3.org/Graphics/Color/sRGB.

[11] Wyszecki, G. and Stiles, W.S. *Color Science: Concepts and Methods, Quantitative Data and Formulae*, New York: John Wiley and Sons, 2000.

[12] Glassner, A.S., *Principles of Digital Image Synthesis*, California: Morgan Kaufman Publishers, 1995.

[13] Ohshita, K. “The World's First Aspherical SLR Lens and Orthographic Projection Fisheye Lens OP Fisheye-NIKKOR 10mm f/5.6”, http://www.nikon.co.jp/main/eng/society/nikkor/n06_e.htm.

[14] Du, H. and Voss, K.J. “Effects of Point-Spread Function on Calibration and Radiometric Accuracy of CCD Camera”, *Applied Optics*, 43(3), 665-670.

[15] Busch, D.D. *Mastering Digital Photography*, Muska & Lipman Publishing, 2004.

[16] CIE, *Methods of Characterizing Illuminance Meters and Luminance Meters: Performance, Characteristics, and Specification*, Publication no. 69, Viena: Central Bureau de la CIE, 1987.